[Short title + Author Name - P&H title] 18 (2025) 106072

Contents lists available at ScienceDirect

Arabian Journal of Chemistry

journal homepage: www.ksu.edu.sa

Original article

β-Sitosterol ameliorates the cognitive deficits and neuropathological hallmarks in an Alzheimer's disease model

Mohd Sajad [a,b], Rafat Ali [c], Rajesh Kumar [b], Nida Jamil khan [c], Shadma Wahab [d], Saad Ali Alshehri [d], Sonu Chand Thakur [a,*]

[a] Center for Interdisciplinary Research in Basic Sciences, Jamia Millia Islamia University, New Delhi 110025, India
[b] Department of Reproductive Bio-Medicine, National Institute of Health, and Family Welfare, Munirka, New Delhi 110067, India
[c] Department of Biosciences, Jamia Millia Islamia University, New Delhi 110025, India
[d] Department of Pharmacognosy, College of Pharmacy, King Khalid University, Abha 61421, Saudi Arabia

ARTICLE INFO

Keywords:
β-sitosterol
Alzheimer's disease
$AlCl_3$
Cholinesterase
Oxidative stress

ABSTRACT

Alzheimer's disease is a neurodegenerative condition causing cognitive decline. Aluminum chloride ($AlCl_3$) is a neurotoxin linked to oxidative stress and neurodegenerative disorders. In light of inadequate current treatments, there is an urgent need for more approaches to treat Alzheimer's disease. β-sitosterol, a phytosterol found in grape skin, fern, and red wine, has potential health benefits. This research aims to assess its preventive impact on $AlCl_3$-induced Alzheimer's disease. The animals were divided into five groups: Group I (control), Group II ($AlCl_3$ 70 mg/kg), Group III (Rivastigmine 2.3 mg/kg), and Groups IV and V (β-sitosterol 50 and 100 mg/kg with $AlCl_3$). $AlCl_3$ was administered from days 5–25, treatments from 26–42 days, and behavioral parameters were measured on days 5, 16, 26, and 42, after which brain samples were collected for the estimation level of oxidative stress, cholinergic function, Glycogen synthase kinase-3β, Rho kinase, Lipoxygenase-5, TNF-α, COX-2, and Na^+K^+ATPase expression and activity. The β-sitosterol prevented cognitive impairment caused by $AlCl_3$ via the reduction of oxidative stress, the improvement of cholinergic function, and the suppression of Glycogen synthase kinase-3β, Rho kinase, Lipoxygenase-5, TNF-α, COX-2, and Na^+K^+ATPase expression and activity. *In silico* studies demonstrated the strong affinity of β-sitosterol towards Alzheimer's disease biomarkers, confirming their function in preventing and regulating its pathogenesis. Consequently, the findings point out that β-sitosterol has an anti-Alzheimer's ability by reducing the toxicity caused by $AlCl_3$.

1. Introduction

Alzheimer's disease (AD) is an insidious and gradually progressing neurodegenerative condition, which is marked by the loss of cognitive abilities of a person, such as learning and memory (Monczor 2005, Johnson et al., 2008). The accumulation of Amyloid-β plaques (Aβ plaques) and neurofibrillary tangles (NFTs) in the brain contributes to AD, leading to a complex neurodegenerative disease. Multiple genes are also linked to AD progression (Dong et al., 2012). Alzheimer's disease is mostly linked to aging, genetic mutations, immunological responses, injuries, medications, hormone replacement therapy, environmental factors, poor nutrition, and lack of social connections (Small 2002). Cholinergic dysfunction, free radical formation, and astrocyte activation are all caused by the production of Aβ plaques and NFT (Sajad et al., 2022). See Table 1..

The most prominent symptoms of AD include cognitive decline, memory loss, recognition problems, speech impairment, and movement problems (Sperling et al., 2011). The accumulation of amyloid plaques in the brain is a key feature of AD. Cognitive damage is primarily caused by the increased breakdown of acetylcholine by the cholinesterase enzyme, resulting in a deficit of acetylcholine in the cerebral cortex (Mohamed et al., 2021). Other enzymes involved in the etiology of AD include glycogen synthase kinase-3β (GSK-3β), catechol-O-methyl transferase (COMT), lipoxygenase-5 (LOX-5), prolyl endopeptidase (PEP), and Rho kinase (ROCK II) (Huang et al., 2008, Siddiqui et al., 2021). These enzymes contribute to AD development, alongside oxidative stress resulting from an imbalance between prooxidant and antioxidant systems (Huang et al., 2016). Both pharmaceutical and non-pharmaceutical treatments have been shown to slow the advancement of AD. Currently, no effective medication exists for AD treatment. AChE

* Corresponding author.
E-mail address: Sthakur@jmi.ac.in (S.C. Thakur).

https://doi.org/10.1016/j.arabjc.2024.106072
Received 1 May 2024; Accepted 19 November 2024
Available online 30 November 2024

Table 1
IC50 values of different antioxidant assays of β-sitosterol against the standard L-AA.

Plant Fractions	*IC_{50} μg/ml ± SD DPPH*	*IC_{50}μg/ml ± SD NO*	*IC_{50} μg/ml ± SD FRAP*	*IC_{50} μg/ml ± SD TRC*
L-AA	25.54 ± 4.0	24.29 ± 0.2	16.13 ± 6.5	4.17 ± 0.3
β-sitosterol	94.17 ± 1.07	26.18 ± 0.57	17.64 ± 0.5	45.41 ± 0.9

inhibitors are the only licensed drugs for managing and treating AD symptoms (Grossberg et al., 2010).

Phytochemicals can improve memory, slow brain aging, and provide therapeutic effects. Research focuses on plants traditionally used in Indian medicine for their effectiveness against various diseases (Farooqui et al., 2018, Andlib et al., 2023). The intraperitoneal injection of $AlCl_3$ causes memory and neurobehavioral impairments in rats by inducing oxidative damage and the accumulation of NFTs and β-amyloids in the hippocampus and cerebral cortex tissues. (Singh and Prashar 2020). $AlCl_3$ has been linked to the development of AD due to its potential neurotoxic effects. It can contribute to oxidative stress, promote the aggregation of amyloid-beta, and disrupt tau protein function, all of which are key pathological features of AD. Additionally, aluminum exposure is thought to impair neurotransmission and induce neuroinflammation, further accelerating the neurodegenerative processes associated with AD (Liaquat et al., 2017, Mousavi-Nasab et al., 2024).

Our research focuses on evaluating the antioxidant and enzyme inhibitory activities of β-sitosterol, a compound derived from the plant extract. β-sitosterol is a bioactive phytosterol with antimicrobial, analgesic, anti-inflammatory, antioxidant, and other beneficial properties (Babu et al., 2020). The compound has been selected based on *in-silico* studies of the plant *Asplenium caudatum.* The anti-Alzheimer's potential of β-sitosterol was assessed *in vivo* against $AlCl_3$-stimulated cognitive damage, cholinergic dysfunction, GSK-3β, LOX-5, ROCK II, Na^+K^+ ATPase, TNF-α, and COX-2 along with the expression of oxidative stress biomarkers in the cerebral cortex and hippocampus tissues of rats.

2. Materials and methods

2.1. Materials

The compounds β-sitosterol, ascorbic acid (L-AA), DPPH, Griess reagent, Ferric chloride, nitro blue tetrazolium chloride (NBT), Sodium Chloride, trichloroacetic acid, Methanol, Aluminium Chloride etc have been purchased from the Sisco Research Laboratories Pvt. Ltd. Maharashtra, India. Potassium ferricyanide and sodium nitroprusside from ADL Enterprises Pvt. Ltd. Elisa Kits has been purchased from the Krishgen Biosystem Company Mumbai India.

2.1.1. Determination of in vitro antioxidant assays

β-sitosterol was evaluated for its antioxidant properties using four *in vitro* methods. L-AA was used as a standard compound.

2.1.1.1. 1,1, diphenyl-2-pacryl hydrazyl (DPPH). The DPPH and Nitric oxide radical scavenging activity was done according to the previously studied methods with slight modifications (Hejazi et al., 2017). Ferric reducing and Total reduction capability assays were also done to ensure the reduction capability of the plant according to previously studied methods (Baba and Malik 2015). L Ascorbate was used as a reference in all antioxidant assays.

2.1.1.2. Nitric oxide radical scavenging activity. The Griess Illosvoy reaction was used to calculate nitric oxide scavenging activity (Babatunde and Kayode 2019, Ahmed et al., 2022). Sodium nitroprusside is decomposed at physiological pH (7.2) in an aqueous solution and generates NO^-. It reacts with oxygen to produce nitrate and nitrite, the quantities of which can be determined using Griess reagent. The naturals products scavenge the nitric oxide by competing with oxygen, thus reducing the level of nitrite ions. For the experiment, sodium nitroprusside (10 mM) in phosphate-buffer saline was mixed with different concentrations (5–320 μg/ml) of β-sitosterol dissolved in water and incubated at 80 ^{0}C for 2 h. After the incubation period, 0.5 ml of Griess reagent (1 % sulphanilamide, 2 % H_3P0_4, and 0.1 % N-(1-naphthyl) ethylenediamine dihydrochloride) was added. The absorbance of the chromophore that formed during diazotization of the nitrite with sulphanilamide and subsequent coupling with Naphthyl-ethylenediamine dihydrochloride was immediately read at 550 nm. Inhibition of nitrite formation by the β-sitosterol and the standard antioxidant ascorbic acid were calculated relative to the control. Inhibition data (percentage inhibition) were linearized against the concentrations of β-sitosterol and standard antioxidant. IC_{50} which is an inhibitory concentration of compound required to reduce 50 % of the nitric oxide formation was calculated.

2.1.1.3. Ferric reducing capability. The ferric reducing power was evaluated as previously described (Baba and Malik 2015). Briefly, different concentrations of compound β-sitosterol (5–360 μg/mL) were mixed with 2.5 mL of phosphate buffer (200 mmol/L, pH 6.6) and 1 % potassium ferricyanide (2.5 mL) followed by incubation at 50 °C for 20 min. The tubes were then centrifuged for 10 min at 10,000 rpm after adding 10 % trichloroacetic acid (2.5 mL). The upper layer (5 mL) was then mixed with distilled water (5.0 mL), followed by 0.1 % of ferric chloride (1 mL). The mixture was allowed to stand for 5 min, and the absorbance was taken at 700 nm using spectrophotometer against the ascorbic acid taken as positive control.

2.2. Animal procurement and housing

Male Wister rats, weighing 200–250 g were used for the experiment and the protocol was approved by the institutional animal ethical committee of the National Institute of Health and Family Welfare, Munirka, New Delhi. The rats were kept in a well-aerated room of 12-hr light and dark cycle using propylene cage (38 × 23 × 10 cm) and husk was used as comforter material. Rats were divided into five groups and each group had 6 animals. No treatment was given to Group I. Group II-$AlCl_3$ was injected intraperitoneally. Group III was received Rivastigmine 2.3 mg/kg. Group IV and V were received β-sitosterol orally at the dose of 50, and 100 mg/kg: respectively, along with $AlCl_3$ injection. The compound β-sitosterol was freshly prepared in distilled water. The injection (i.p) of $AlCl_3$ was given from the 5th to 25th day and treatment with compound (orally) was started on the 26th day after the $AlCl_3$ injection and continued till the 42nd day of the experiment. The behavioral parameters were performed on the 5th, 16th, 26th, and 42nd days of the experiment. On the 42nd day, the animals were sacrificed, and brain samples were taken out for estimation of cholinergic biomarkers (acetylcholinesterase and butyrylcholinesterase) and Rho kinase (ROCK II) expression, glycogen synthase kinase-3, lipoxygenase, Na^+K^+ ATPase and TNF-α and COX-2 expression. oxidative stress parameters (glutathione, malondialdehyde, nitric oxide levels and superoxide dismutase activity).

2.2.1. Estimation of behavioral parameters

The spatial memory test of animals was analysed followed the method of Morris water maze (Morris 1984). Four quadrants of equal size have been made in water tank (1, 2, 3, and 4) and a resting platform was set into 4th quadrant. During the first four days i.e., acquisition sessions, the animals has been trained to escape themselves from water. The animals were trained by placing them in each quadrant, keeping the platform at the same point during the series of trails. The preliminary trail was finished precipitously once the rat got to the stage or while 120 s had passed. After that the rat who got the platform on time was allowed

to remain on it for 5 s, while the other one was guided gently towards platform and allowed to sit there for 5 s. After the completion of each trial, the rats were softly wiped and dried with a towel and placed to their subsequent cages. Spatial probe trail of 60 s was conducted on 5th day to evaluate the spatial memory. The same procedure was followed on 16th, 26th, and 42nd day of experiment to detect the memory of experimental rats. The time taken by each rat to escape itself was noted in seconds.

2.2.2. Analysis of urine and serum

The level of creatinine, uric acid, phosphatase and urea, was studied according to (Nirala et al., 2019). Urine was collected on the last day of experiment by keeping the rats in metabolic cages for 24-hour on the 42nd day. Animals have been allowed free access to drinking water during the urine collection period. A drop of concentrated hydrochloric acid was used for urine preservation and stored at 4 °C. The urine was analysed for urea, uric acid, phosphatase, and creatine level by kit Randox laboratories (India) Pvt. Ltd. On the 43rd day, the blood was collected from the *retro*-orbital sinus under mild anaesthesia with diethyl ether. Blood was centrifuged at 15,000 rpm for 20 min to get the serum for the analysis of creatinine, uric acid, phosphatase, and urea. (Kit Randox laboratories (India) Pvt. Ltd).

2.3. Biochemical estimation

Upon completion of final behavioral tests on 42nd day, the animals were decapitated under ether anaesthesia followed by cervical dislocation and the brain samples were quickly removed from rats and kept over a glass plate placed on ice, and then dissected into the hippocampus and cerebral cortex according to (Mehla et al., 2012) and stored at −80 °C till further analysis within next 7 days.

2.3.1. Tissue preparation

Hippocampus and cerebral cortex samples were thawed and homogenized in 10 % (w/v) ice–cold 0.1 M phosphate buffer (pH 7.4) for estimation of cholinesterase enzymes, oxidative stress parameters, and the level of other biomarkers such as Rho kinase (ROCK II) expression, glycogen synthase kinase 3, lipoxygenase, Na^+K^+ ATPase and TNF-α and COX-2. Lysis buffer was used to homogenise the hippocampus and cerebral cortex samples for the estimation of expression of ROCK II.

2.3.2. Enzyme inhibitory activity

2.3.2.1. Acetylcholinesterase and butyrylcholinesterase inhibitory activity. The level of cholinergic biomarkers, AChE and BuChE was assessed at 450 nm by following the method described by (Ellman et al., 1961) and Krishgen biosystem (Mumbai India).

2.3.2.2. Inhibitory effect of glycogen synthase kinase-3β (GSK-3β). The level of GSK-3β was estimated at 450 nm by following the procedure provided along with rat ELISA kits by Krishgen Biosystem Company (Mumbai, India).

2.3.2.3. Inhibitory effect of Rho kinase (ROCK II). The level of Rho kinase (ROCK II) was estimated at 450 nm by following the procedure provided along with rat ELISA kits by Krishgen Biosystem Company (Mumbai, India).

2.3.2.4. Lipoxygenase (LOX) inhibitory activity. The level of *Lipoxygenase (LOX)* was estimated at 450 nm by following the procedure provided along with rat ELISA kits by Krishgen Biosystem Company (Mumbai, India).

2.3.2.5. Assessment of Na^+K^+ ATPase level. The level of Na^+K^+ ATPase was estimated at 450 nm by following the procedure provided along with rat ELISA kits by Krishgen Biosystem Company (Mumbai, India).

2.4. Measurement of oxidative stress

2.4.1. Lipid peroxidation estimation

The estimation of MDA (Malondialdehyde) was carried out by the previously described method (Ohkawa et al., 1979). The AR-grade reagents were used as procured. 1.5 ml of acetic acid, pH 3.5 (20 % v/v), thiobarbituric acid 1.5 ml (0.8 % w/v), and Sodium dodecyl sulfate 0.2 ml (8.1 % w/v) was added to processed tissue sample of 0.1 ml, and the mixture was heated for 1 h at 90 ^{0}C. The reaction mixture was cooled by employing tap water by subsequent addition of 15:1 ratio of n-butanol/pyridine (5 ml) and doubly distilled water 1 ml and vortexed. Then the mixture was centrifuged for 10 min at 5000 rpm. The supernatant organic layer was separated, and absorbance was taken by utilizing spectrophotometer at 532 nm.

2.4.2. Reduced glutathione estimation

(Ellman and biophysics 1959) method was applied for the estimation of reduced glutathione (GSH). Equivalent amount of tissue homogenate and trichloro acetic acid 10 % were mixed and centrifuged to separate the proteins. 2.0 ml of phosphate buffer (0.3 M) (pH 8.4), 5,5-dithiobis (2-nitrobenzoic acid) 0.5 ml were added to 0.1 ml of supernatant followed by the addition of 0.4 ml distilled water and vortexed. The absorbance was measured at 412 nm.

2.4.3. Superoxide dismutase (SOD) estimation

The calculation of SOD was carried out according to (Marklund and Marklund 1974). 4 mM of pyrogallol (0.05 ml) was mixed with 0.9 ml of buffer followed by the addition 0.05 ml of homogenate sample. Absorbance was measured at 420 nm.

2.4.4. Nitric oxide (NO) estimation

(Green et al., 1982) method was employed to determine the NO level by using Griess reagents. Subsequently 500 µl of supernatant tissue and Griess reagents 500 µl was used to determined nitrite level. The mixture was incubated at room temperature for 10 min, and the absorbance was taken at 520 nm.

2.4.5. Estimation of catalase

Catalase enzymes break the H_2O_2 (hydrogen peroxide) into H_2O and O_2 by using manganese/iron as a cofactor during the process. This assay was performed according to (Singh and Prashar, 2020). Briefly, 10 % w/v 0.05 ml of supernatant was added into 1.95 ml of 0.05 M phosphate buffer (pH 7). Then 1 ml of H_2O_2 (0.019 M) was added and absorbance was measured at 240 nm for 30 sec.

2.5. Histopathological studies

For histopathology, the cerebral cortex and hippocampus of rat's brains were fixed in 4 % paraformaldehyde and then placed in paraffin. These specific tissues were sliced into 5 mm pieces using a section cutter (Leica, Germany) and stained using haematoxylin and eosin. These slides were examined using a light microscope.

2.6. Molecular dynamic study

The X-ray crystallographic structures of AD associated biomarkers (receptor proteins) i.e., rock-II, GSK-3β, AChE, BChE, and LOX-5 (PDB ids: 4L6Q, 4 nm3, 4PQE, 6ESY, and 6N2W respectively) were retrieved from the protein data bank (PDB) having resolutions 2.79 A°, 2.1 A°, 2.9 A°, 2.8 A°, and 2.71 A° respectively. The loop modelling of these missing residues (as seen in their respective REMARK 465 line) done in MODELLER 10.2 and the predicted models evaluated in ProSA & SAVESv6.0 and minimized in Modrefiner. Further, molecular docking study of compound β-sitosterol was carried out for proteins Rock-II, GSK-3β,

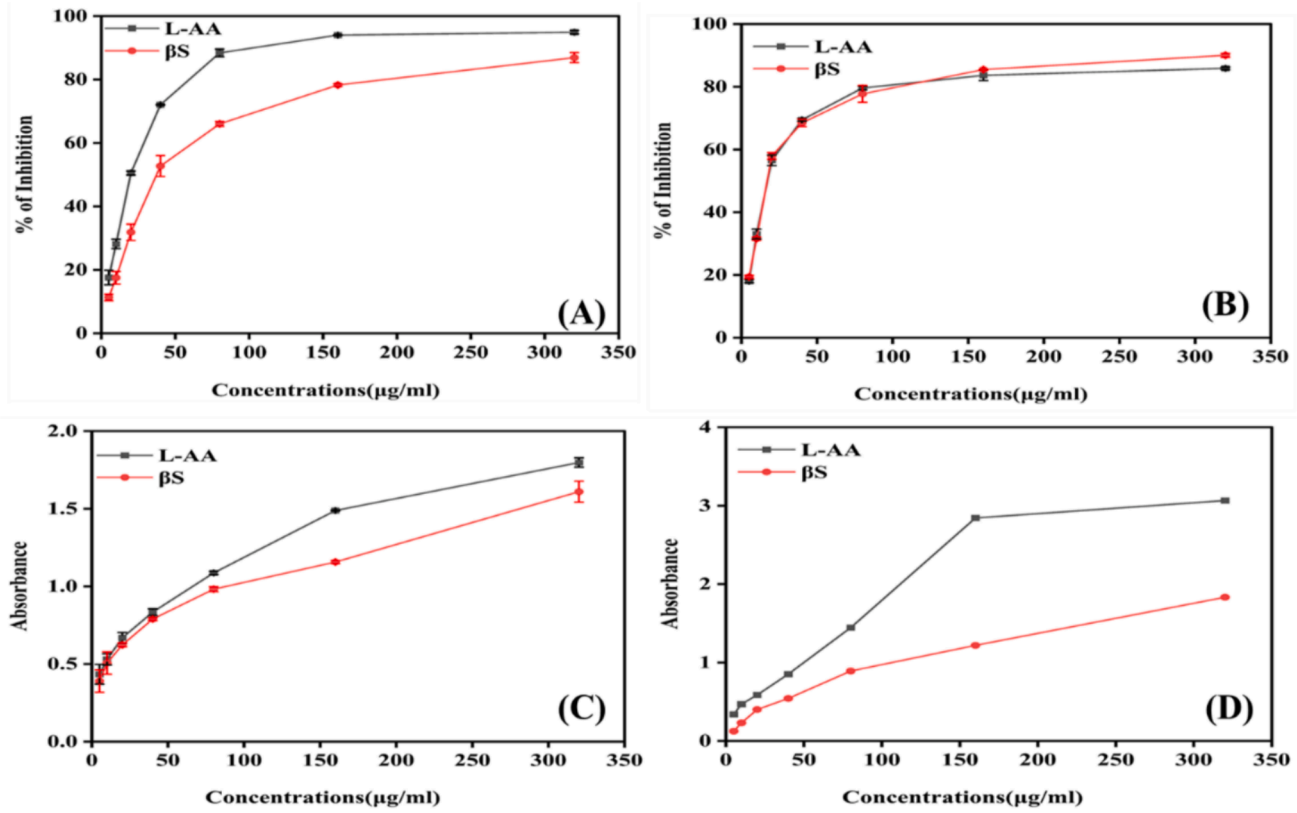

Fig. 1. *In vitro* antioxidant activities (A) DDPH, (B) Nitric oxide scavenging, (C) Ferric Reducing Capability and (D) Total antioxidant capability in concentration-dependent manner. L-ascorbic acid is taken as control. All the assays are performed in triplicate and the results are expressed as mean standard deviation (SD).

AChE, BuChE, and LOX-5 using AutoDock 4.2 and AutoDock vina (Trott and Olson 2010). 3D-structure of docked complexes analyzed for H-bonds in the PyMOL and 2D & 3D-interaction plots visualization and analysis done using a free version of BIOVIA Discovery Studio Visualizer and PyMOL.

2.7. Molecular dynamics simulation

The molecular dynamics investigation of compound β-sitosterol was done to perform all-atom MD simulations at 300 K through the GROMACS simulation suite (Abraham et al., 2015). The Charmm27 force-field was employed to simulate the LOX-5 (6N2W) system in ligand-bound and apo states with β-sitosterol. The topology and force field parameters for β-sitosterol were generated using the CGenFF webserver.

Table 2
The behavioural study of experimental rats of individual groups on different days.

	ESCAPE LATENCY TIME in Sec			
	5th day	*16th day*	*26th day*	*42nd day*
Group I, 0.9 % w/v NaCl 10 ml/kg; p.o.	19.3 ± 2.5	15.43 ± 1.4	7.33 ± 1.5	3.1 ± 0.1
Group II $AlCl_3$ 70 mg/kg; i.p + 0.9 % w/v NaCl 10 ml/kg; p.o	23.00 ± 3.6	49.33 ± 3.5	60.0 ± 0.0	60.0 ± 0.0
Group III $AlCl_3$ 70 mg/kg; i.p + rivastigmine 2.5 mg/kg; p.o	25.66 ± 2.3	53.0 ± 4.0	60.0 ± 6.0	20.06 ± 4.2
Group IV $AlCl_3$ 70 mg/kg; i.p + β-sitosterol −50 mg/kg; p.o	21.33 ± 1.5	57.0 ± 0.0	58.66 ± 2.3	23.16 ± 3.3
Group V $AlCl_3$ 70 mg/kg; i.p + β-sitosterol −100 mg/kg; p.o	20.33 ± 1.5	54.33 ± 1.7	59.33 ± 2.7	14.83 ± 3.6

Each system was centralized in a cubic box of 10 Å distance to the edges. Solvation in an aqueous environment facilitated by the addition of water molecules through the SPC216 model. The appropriate amount of counterions incorporated to maintain the charge neutrality of the systems. The steepest descent algorithm used to perform the energy minimization followed by position restraint procedure with NVT and NPT ensembles for all systems. Ultimately, the generated trajectory was examined in the GROMACS' built-in tools after each system underwent a 100 ns simulation.

3. Results

3.1. Determination of in vitro antioxidant assays

3.1.1. DPPH free radical scavenging activity

The ability of β-sitosterol to scavenge the DPPH free radicals was calculated by determining the competency to reduce the stable radical generated by DPPH. Although the compound β-sitosterol was found to be as substantial as L-Ascorbate. Results presented in Fig. 1A shows that β-sitosterol inhibited DPPH radicals in a dose-dependent manner with an IC_{50} value of (94.17 ± 1.07 µg/ml) as compared to L-AA (24.54 ± 4.0 µg/ml).

3.1.2. Nitric oxide radical scavenging activity

The scavenging activity of standard L-AA, and β-Sitosterol with respect to IC_{50} values are 24.29 ± 0.2 and 26.18 ± 0.57, respectively ($p < 0.0001$) (Fig. 1B). In addition, it was discovered that β-sitosterol considerably decreased the amount of nitrite generated by the breakdown of sodium nitroprusside like L-AA showed it potential antioxidant properties.

3.1.3. Ferric reducing capability

In this experiment, the capacity of phytocompound β-sitosterol to

Table 3
The levels of urea, uric acid, and creatinine were studied in serum and urine of experimental rats.

Groups	Samples					
	Urine			Serum		
	Urea	*Uric acid*	*Creatinine*	*Urea*	*Uric acid*	*Creatinine*
G-I (Control)	22.25 ± 0.07	4.10 ± 0.006	0.52 ± 0.02	23.07 ± 0.01	2.06 ± 0.01	0.50 ± 0.03
G-II (Diseased)	67.49 ± 0.51	12.84 ± 0.01	1.26 ± 0.01	60.61 ± 0.02	4.16 ± 0.05	1.11 ± 0.06
G-III (Rivastigmine)	25.83 ± 0.13	5.35 ± 0.05	0.54 ± 0.02	22.58 ± 0.09	3.04 ± 0.04	0.54 ± 0.02
G-IV (β-sitosterol −50)	34.87 ± 0.17	4.73 ± 0.07	0.60 ± 0.01	33.63 ± 0.01	3.25 ± 0.03	0.58 ± 0.04
G-V (β-sitosterol-100)	25.94 ± 0.03	2.87 ± 0.07	0.55 ± 0.01	24.53 ± 0.08	2.97 ± 0.09	0.52 ± 0.01

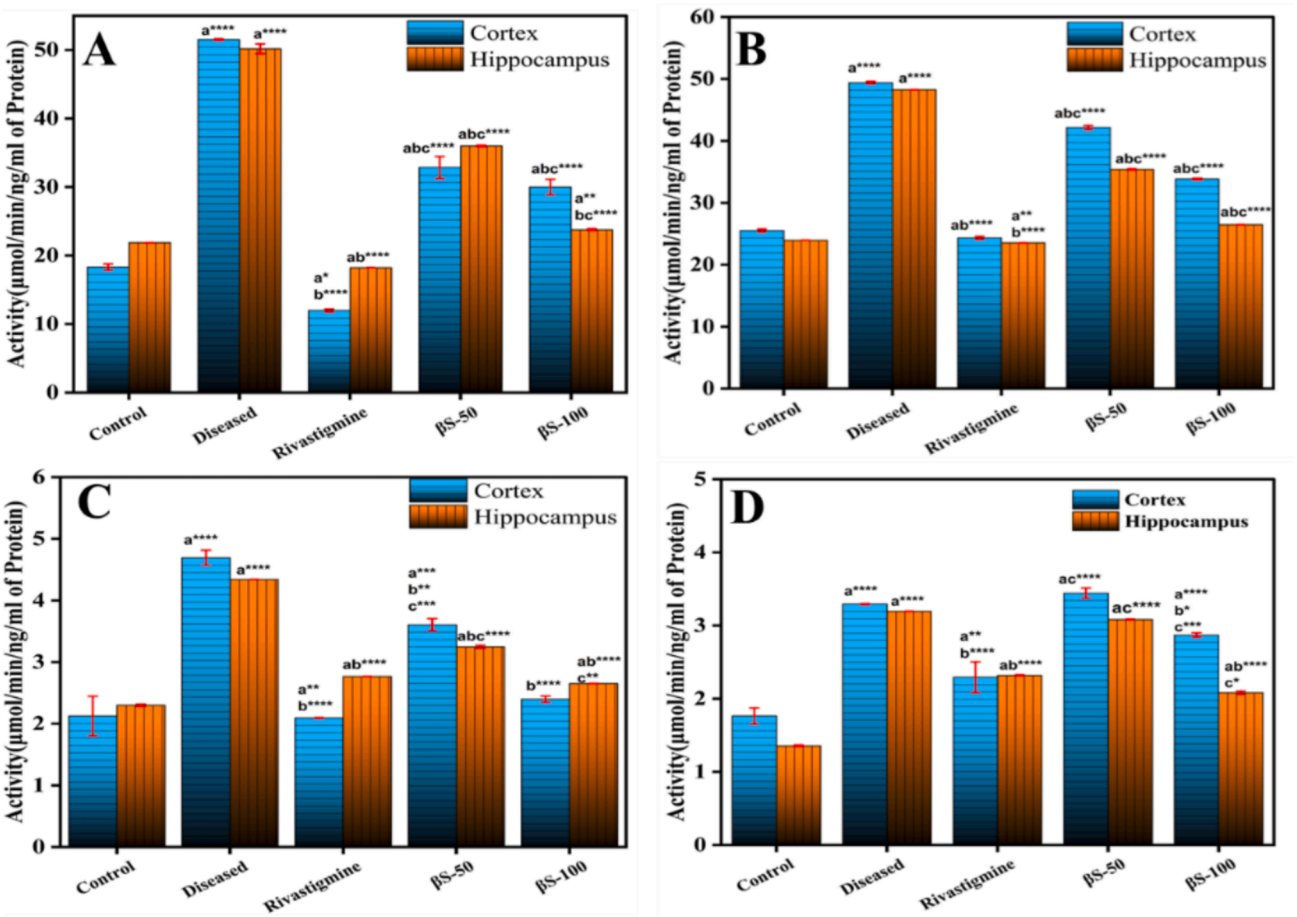

Fig. 2. Effect of β-sitosterol (50 and 100 mg/kg) on the level of (A) AChE, (B) BuChE, (C) GSK-3β and (D) LOX-5 in cerebral cortex and hippocampus regions of $AlCl_3$ induced AD model. Data is represented as mean ± S. D of means. *p < 0.05, **p < 0.01, ***p < 0.001; ****p < 0.0001as compared to control (a), diseased (b) and $AlCl_3$ + rivastigmine (c).

reduce ferric iron was measured. The absorbance at 700 nm was drastically altered by increasing concentrations of compound, with IC50 values of L-AA 16.13 ± 6.5 and β-sitosterol 17.64 ± 0.5, respectively (Fig. 1C).

3.1.4. Total reducing capability assay

When represented as absorbance values, the reducing power of L-AA and β-sitosterol were 3.06 ± 0.003, and 1.83 ± 0.2 at 320 µg/ml (Fig. 1D). The IC_{50} values were 4.17 ± 0.3 45.41 ± 0.93 µg/ml for L. AA and β-sitosterol, respectively. The reducing capacity is a strong indicator of its potential antioxidant effect of phytochemicals. The concentration-dependent high inhibition efficiency of β-sitosterol shows that it can lower the transition state of iron and, in turn, the amount of superoxide and hydroperoxyl radicals formed.

3.2. In vivo study

3.2.1. Effect on Morris water maze test

See Table 2..

3.2.2. Effect on urine and serum

The level of different biomarkers, such as urea, uric acid, and creatinine, in urine and serum has been studied, and the results are demonstrated in Table 3, respectively.

3.2.3. Effect on the activity of AChE in cerebral cortex and hippocampus

The level of AChE activity was enhanced significantly ($p < 0.0001$) from 18.32 ± 0.41 activity/ng of protein in cerebral cortex and 21.88 ± 0.007 activity/ng of protein in hippocampus of normal group to 51.51

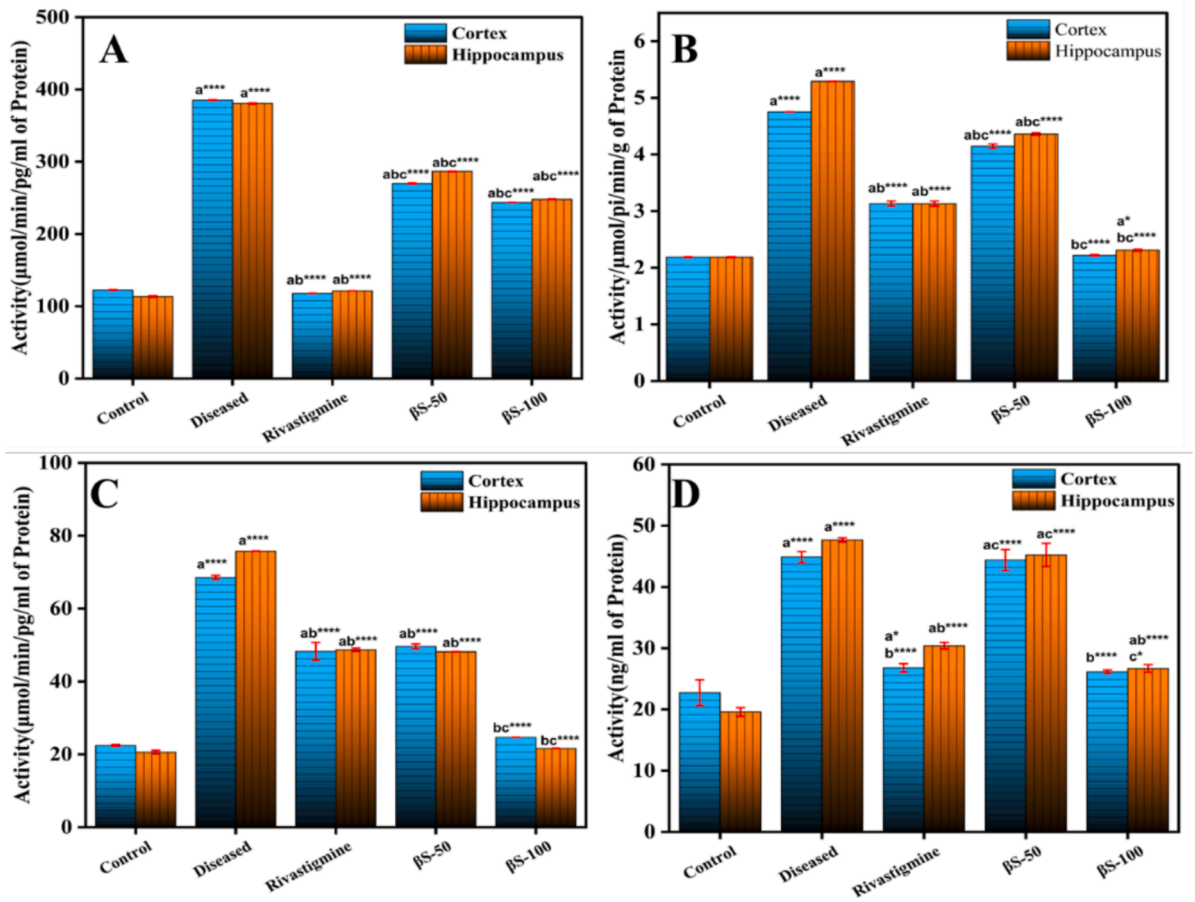

Fig. 3. Effect of β-sitosterol (50 and 100 mg/kg) on the level of (A) Rho-II, (B) Na^+K^+ATPase, (C) TNF-α and (D) COX-2 in cerebral cortex and hippocampus regions of $ALCl_3$ induced AD model. Data is represented as mean ± S. D of means. *p < 0.05, **p < 0.01, ***p < 0.001; ****p < 0.0001as compared to control (a), diseased (b) and $AlCl_3$ + rivastigmine (c).

± 0.5 and 50.17 ± 0.7 activity/ng of protein in cerebral cortex and hippocampus of diseased group, respectively (Fig. 2A). A substantial decline in the level of AChE activity was detected with β-sitosterol at doses of 50 mg/kg (32.85 ± 1.6; $p < 0.0001$), and 100 mg/kg (29.98 ± 1.1; $p < 0.0001$), in cerebral cortex and 50 mg/ kg (36.01 ± 0.01; $p < 0.0001$), and 100 mg/kg (23.77 ± 0.13; $p < 0.002$) in hippocampus regions, as compared to diseased and normal groups, respectively.

3.2.4. *Effect on the activity of BuChE in cerebral cortex and hippocampus*

The activity of BuChE was enhanced significantly ($p < 0.001$) from 25.51 ± 0.2 activity/ng of protein in cerebral cortex and 23.9 ± 0.007 activity/ng of protein in hippocampus region of normal group to 49.39 ± 0.20 and 48.26 ± 0.009 /ng protein in cerebral cortex and hippocampus of diseased group, respectively (Fig. 2B). A substantial decline in the activity of BuChE level was examined in cerebral cortex with β-sitosterol at doses of 50 mg/kg, (42.14 ± 0.31; $p < 0.0001$) and 100 mg/kg (33.83 ± 0.14; $p < 0.0001$). In hippocampus, substantial decline in the activity of BuChE was also seen with β-sitosterol at 50 mg/kg, 35.39 ± 0.09, and 100 mg/kg 26.48 ± 0.009 ($p < 0.0001$), compared to normal group, respectively.

3.2.5. *Effect on the activity of GSK-3β in cerebral cortex and hippocampus*

The expression of GSK-3β increased substantially ($p < 0.001$) was observed from 2.12 ± 0.3 activity/ng of protein in cerebral cortex and 2.29 ± 0.09 activity/ng of protein in hippocampus of normal control group to 4.69 ± 0.12 and 4.34 ± 0.001 activity/ng of protein in cerebral cortex and hippocampus of $AlCl_3$ treated group, respectively (Fig. 2C). A significant decline in the activity of GSK-3β was seen in cerebral cortex with β-sitosterol at doses of 50 mg/kg (3.60 ± 0.09; $p < 0.0006$), and 100 mg/kg (2.39 ± 0.04; $p < 0.0001$) and in hippocampus at doses of 50 mg/kg (3.24 ± 0.02; $p < 0.0001$), and 100 mg/kg (2.65 ± 0.002; $p < 0.0001$), compared to diseased and normal groups, respectively.

3.2.6. *Effect on lipoxygenase-5 activity (LOX-5) in cerebral cortex and hippocampus*

The activity of LOX-5 has been enhanced significantly ($p < 0.001$) from 1.76 ± 0.11 activity/ng of protein in cerebral cortex and 1.35 ± 0.01 activity/ng of protein in hippocampus of normal group to 3.29 ± 0.009 and 3.19 ± 0.001 activity/ng of protein in cerebral cortex and hippocampus of diseased group, respectively (Fig. 2D). Moreover, a significant decline in LOX-5 activity was detected in cerebral cortex with β-sitosterol treatment at doses of 50 mg/kg (3.44 ± 0.07; $p < 0.0001$), and 100 mg/ kg (2.87 ± 0.02; $p < 0.0001$) and in hippocampus at doses of 50 mg/kg (3.04 ± 0.004; $p < 0.0001$), and 100 mg/ kg (2.08 ± 0.02; $p < 0.0001$), compared to normal group, respectively.

3.2.7. *Effect on the activity of Rho-II in cerebral cortex and hippocampus*

The activity of Rho-II was raised substantially ($p < 0.001$) from 122.28 ± 0.62 activity/ng of protein in cerebral cortex, and 113.42 ± 0.35 activity/ng of protein in hippocampus region of normal group to 385.16 ± 0.55 and 380.65 ± 0.88 activity/ng of protein in cerebral cortex and hippocampus region of diseased group, respectively (Fig. 3A). Moreover, a significant decline in the activity of Rho-II was detected in cerebral cortex with β-sitosterol treatment at 50 mg/kg, 259.80 ± 0.76 activity/ng of protein, and 100 mg/ kg, 243.51 ± 0.02 activity/ng of protein ($p < 0.0001$) dose concentrations, and in hippocampus, 286.59 ± 0.36 activity/ng of protein at dose of 50 mg/kg ($p <$

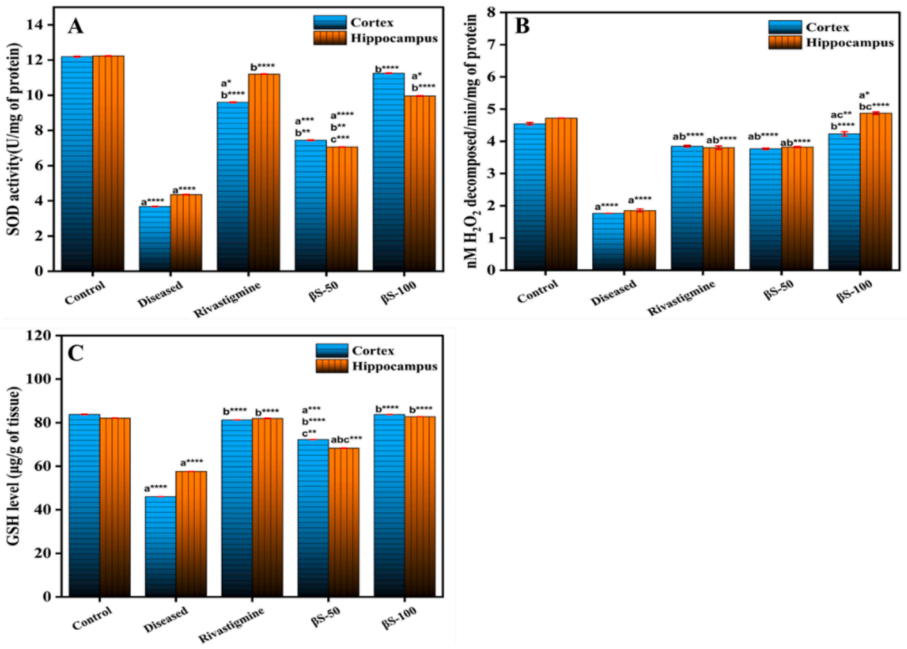

Fig. 4. Effect of β-sitosterol (50 and 100 mg/kg) on the level of (A) SOD, (B) Catalase, and (C) GSH in CC and HPC regions of $ALCl_3$ induced AD model. Data is represented as mean ± S. D of means. *p < 0.05, **p < 0.01, ***p < 0.001; ****p < 0.0001as compared to control (a), diseased (b) and $AlCl_3$ + rivastigmine (c).

0.0001), and 248.22 ± 0.34 activity/ng of protein at dose of 100 mg/kg, (p < 0.0001), respectively compared to diseased and control groups.

3.2.8. *Effect on the Na^+K^+ ATPase activity*

Fig. 3B demonstrates the effect of oral administration of β-sitosterol on the activity of Na^+K^+ATPase in brain tissue. It has been investigated that the level of Na^+K^+ATPase activity increased in the $AlCl_3$ treated group 4.75 ± 0.001 and 5.29 ± 0.001 from normal group 2.18 ± 0.08 and 2.18 ± 0.001 in the cerebral cortex and hippocampus regions respectively (Fig. 3B). Subsequently, after treatment with β-sitosterol at 50 mg/kg (4.14 ± 0.03, p < 0.0001), and 100 mg/kg (2.21 ± 0.01, p < 0.0001) in the cerebral cortex and 50 mg/kg (4.36 ± 0.02, p < 0.0001), and 100 mg/kg (2.30 ± 0.01, p < 0.04) in hippocampus regions, has significantly reduced the Na^+K^+ATPase activity, compared to normal and $Alcl_3$ treated groups. This is because β-sitosterol enhances cholinergic function, which is essential for the formation and recall of memories, the acquisition of new information, and the regulation of motor activity in the brain.

3.2.9. *Effect on the expression of TNF-α and Cox-2 in cerebral cortex and hippocampus*

A significant (p < 0.001) increase in TNF-α and Cox-2 activity was observed from 22.43 ± 0.26 and 22.72 ± 2.11 activity/ng of protein in cerebral cortex and 20.62 ± 0.46 and 19.58 ± 0.59 activity/ng of protein in hippocampus to 68.53 ± 0.56 and 44.87 ± 0.91 activity/ng of protein in cerebral cortex and 75.78 ± 0.03 and 47.68 ± 0.33 activity/ng of protein in hippocampus of diseased group ($AlCl_3$ treated), respectively (Fig. 3C and 3D). Significant decrease in TNF-α and Cox-2 level was observed in cerebral cortex with β-sitosterol compound treatment at doses of 50 mg/kg 49.63 ± 0.67 and 44.37 ± 1.72 (p < 0.0001), and 100 mg/kg 24.64 ± 0.05 and 26.12 ± 0.30 (p < 0.0001) compared to control, and $AlCl_3$ treated groups, respectively. In hippocampus, significant decrease in the level of TNF-α and Cox-2 was also observed with β-sitosterol at 50 mg/kg 48.18 ± 0.03 and 45.24 ± 1.8 (p < 0.0001), and 100 mg/kg 21.64 ± 0.05 and 26.69 ± 0.62 (p < 0.0001), compared to control and diseased groups, respectively.

3.3. *Oxidative stress study*

3.3.1. *SOD activity in cerebral cortex and hippocampus*

There is a significant decrease in the activity of SOD (p < 0.001) from 69.63 ± 2.75 % and 68.25 ± 2.96 % in cerebral cortex and hippocampus regions of normal control group to 47.67 ± 3.97 % and 45.33 ± 4.13 % in cerebral cortex and hippocampus of $AlCl_3$ treated group, respectively (Fig. 4A). The OF-W fraction at the dose of 50 and 100 mg/kg has substantially prevented the reduction of SOD activity in both regions as compared to diseased group (p < 0.05 and p < 0.001, respectively). Moreover, the treatment with OF-M50 and OF-M100 mg/kg has also enhance the activity of SOD in cerebral and hippocampus regions respectively as compared to $AlCl_3$ treated group.

3.3.2. *Effect on the level of catalase activity in cerebral cortex and hippocampus*

The level of catalase was found to be 4.54 ± 0.04 and 4.71 ± 0.001 μM of H_2O_2 decomposed/ min/mg of protein in cerebral cortex and hippocampus regions. $AlCl_3$ treatment resulted in a significant decrease to 1.76 ± 0.003 and 1.85 ± 0.04 (p < 0.0001) in catalase level in both regions, compared to normal group, respectively (Fig. 4B). Moreover, β-sitosterol causes an increase in catalase level at 50 mg/kg, and 100 mg/kg dose concentrations, (3.76 ± 0.02p < 0.0001 and 4.23 ± 0.06p < 0.003) in cortex and (3.82 ± 0.01p < 0.0001, and 4.87 ± 0.03p < 0.03) in hippocampus region, compared to diseased and normal groups, respectively.

3.3.3. *Effect on the level of GSH in cerebral cortex and hippocampus*

The level of GSH was substantially (p < 0.0001) reduced from 83.79 ± 0.14 μg/g tissue in cerebral cortex and 82.12 ± 0.01 μg/g tissue in hippocampus of normal group to 46.01 ± 0.01 μg/g tissue in cerebral cortex and 57.67 ± 0.002 μg/g tissue in hippocampus of $Alcl_3$ treated group ((Fig. 4C)). The GSH level was significantly enhanced from 46.01 ± 0.01 μg/g tissue in cerebral cortex, and 57.67 ± 0.002 μg/g tissue in hippocampus in diseased group to 72.20 ± 0.01 (p < 0.0004), and 83.76 ± 0.00 (p < 0.0001) in cerebral cortex, and 68.31 ± 0.01 (p < 0.0002), and 82.73 ± 0.01 μg/g tissue (p < 0.0001), in hippocampus at the dose of β-sitosterol 50, and 100 mg/kg treated groups, respectively.

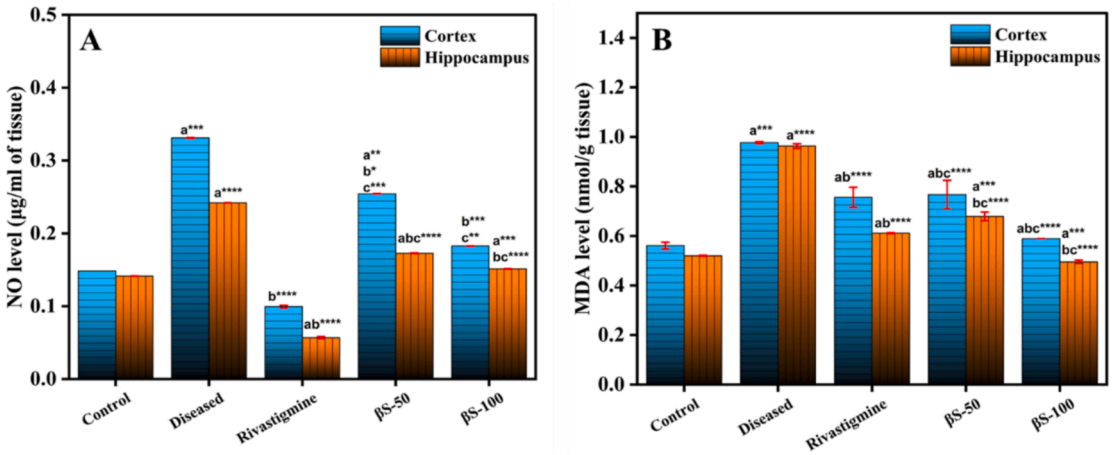

Fig. 5. Effect of β-sitosterol (50 and 100 mg/kg) on the level of (A) Lipid peroxidation and (B) Nitric oxide in CC and HPC regions of $ALCl_3$ induced AD model. Data is represented as mean ± S. D of means. *p < 0.05, **p < 0.01, ***p < 0.001; ****p < 0.0001as compared to control (a), diseased (b) and $AlCl_3$ + rivastigmine (c).

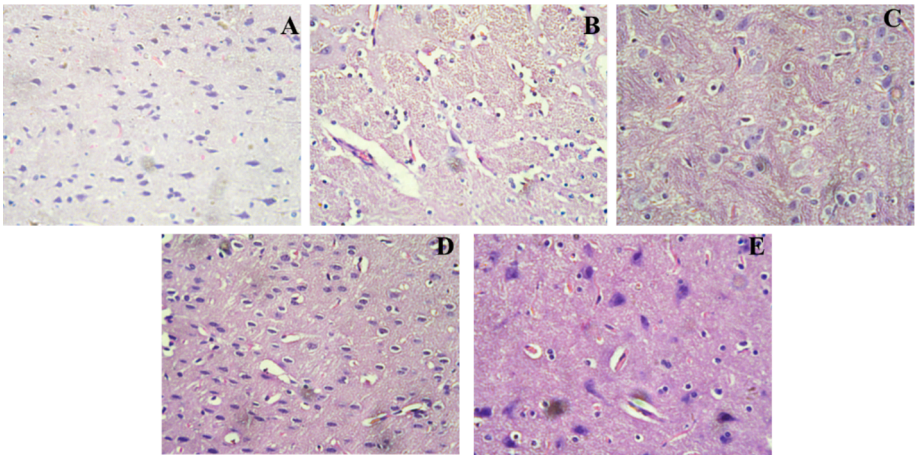

Fig. 6. Histopathology of the Cerebral Cortex region in rat brain; A (control group): Regular histological features and well developed neurons; B (Diseased group): neuronal dysfunction with irregular cellular morphology treated with $AlCl_3$, C (Rivastigmine (2.3 mg/kg) treated group): less histopathological alterations were observed; D (βS-50 mg/kg) and E (βS-100 mg/kg): showed significant recovery after treatment as compared to diseased group.

3.3.4. Effect on lipid peroxidation (MDA) level in cerebral cortex and hippocampus

The level of lipid peroxidation (MDA) was increase ($p < 0.001$) in the cerebral cortex (0.97 ± 0.003 nmol/g tissue) and hippocampus regions (0.96 ± 0.009 nmol/g tissue) of diseased group, comparable to normal group (0.56 ± 0.01 and 0.52 ± 0.002 nmol/g tissue), respectively, (Fig. 5A). The compound β-sitosterol at the doses of 50 mg/kg 0.76 ± 0.05 and 100 mg/kg 0.58 ± 0.00 ($p < 0.0001$) in cerebral cortex, and 50 mg/kg 0.67 ± 0.01($p < 0.0008$) and 100 mg/kg 0.49 ± 0.00 ($p < 0.0004$) in hippocampus region, substantially decreased the level of MDA of brain, compared to diseased and normal groups.

3.3.5. Effect on the level of nitric oxide (NO) in cerebral cortex and hippocampus

The nitrite, a sign of NO level in cells was significantly raised ($p < 0.001$) from 0.15 ± 0.002 µM/g tissue in cerebral cortex and 0.14 ± 0.00 µM/g tissue in hippocampus of normal control group to 0.33 ± 0.0 µM/g tissue and 0.24 ± 0.01 µM/g tissue in cerebral cortex and hippocampus of diseased group (Fig. 5B). The treatment with compound β-sitosterol substantially decreased the level of nitrite in cerebral cortex at doses 50 mg/kg, 0.25 ± 0.02 µM/g, ($p < 0.003$), and 100 mg/kg 0.18 ± 0.00 µM/g ($p < 0.0007$), compared to diseased group, respectively. The level of nitrite was also reduced significantly in hippocampus tissue with compound β-sitosterol at the doses of 50 mg/kg, 0.17 ± 0.002 µM/g ($p < 0.0001$), and 100 mg/kg, 0.15 ± 0.00 µM/g ($p < 0.0002$), compared to control group, respectively.

3.4. Histopathological study

Histological findings of the cerebral cortex and hippocampus of rats (Figs. 6 and 7) revealed extensive changes, including the loss of neurons and aberrant shape of cells, in the Alcl3-treated group as compared to the normal control group (0.9 %NaCl). After the treatment with the compound β-sitosterol at the dose of β-sitosterol-50, and β-sitosterol-200 mg/kg reduces the alterations and morphology of cells.

3.5. In silico studies

3.5.1. Molecular docking-based virtual screening

The 2-D compound library of compound β-sitosterol was downloaded from PubChem database and minimized and saved in 3-D in PyRx software and virtual screening was performed for discovering effective inhibitors against the AD associated biomarkers using AutoDock 4.2 tool and AutoDock Vina command line interface. The projected docking score (−8.6 to −11.6 kcal/mol) were retrieved against each protein, and their interactive binding site residues were visualized in PyMol and figures were generated using Discovery Studio (Table 4).

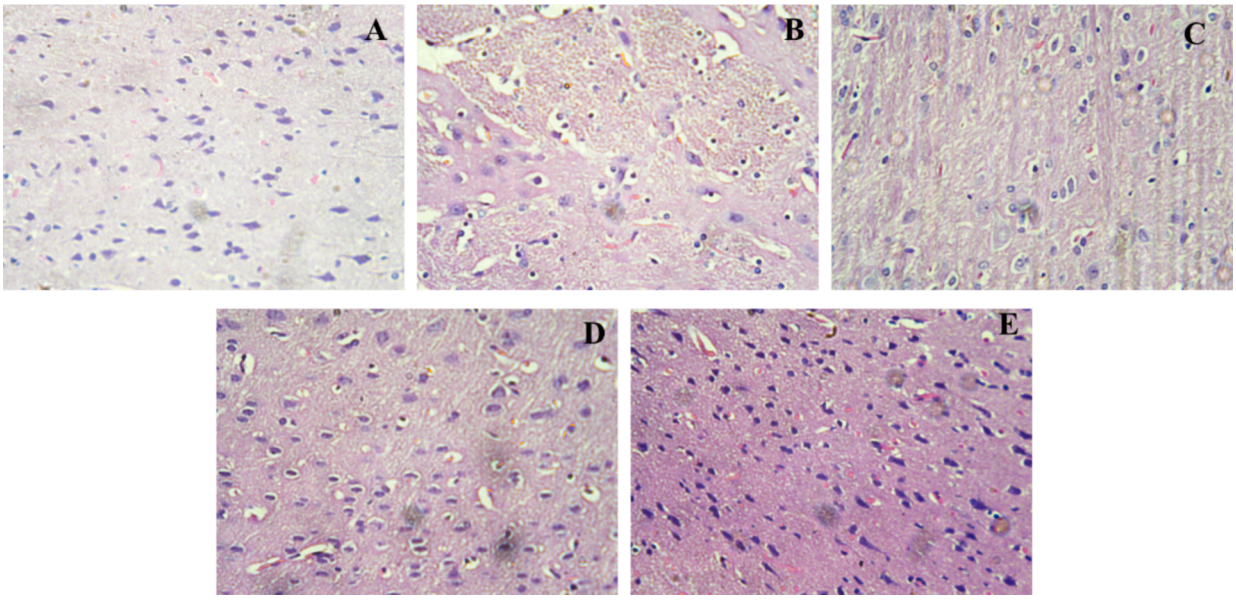

Fig. 7. Histopathology of the Hippocampus region in rat brain; A (control group): Regular histological features and well developed neurons; B (Diseased group): neuronal dysfunction with irregular cellular morphology treated with $AlCl_3$, C (Rivastigmine (2.3 mg/kg) treated group). less histopathological alterations were observed; D (βS-50 mg/kg) and E (βS-100 mg/kg). showed significant recovery after treatment as compared to diseased group.

Table 4
Binding affinity of top compound β-Sitosterol with their respective AD proteins.

S. No.	Compound	Binding affinity (Kcal/mol)					
		Proteins	AChE	BuChE	LOX	GSK-3β	Rho-II
		PDB ids	4PQE	6ESY	6N2W	4 nm3	4L6Q
1	beta-sitosterol	−8.6		−9.1	−9.8	−8.6	−8.0
2	Rivastigmine	−7.1		−6.1	−5.7	−6.2	−7.1

3.5.2. Analysis of interactions

The docking results of compound β-sitosterol against AD biomarkers shows that β-sitosterol has highest binding affinity −9.8 Kcal/Mol against proteins 6N2W with binding site residues Phe634, Trp219, Asp221, Phe222, Met637, Ala223, Phe225, Phe224, Glu630, Gln627, Ser233, Ile232, Lys231, Val230, Phe628 and Arg684. β-sitosterol forms H-bonds with Pro136 of 4NM3 and Asp221 of 6N2W. The binding affinities against the specific receptor proteins have been shown in Fig. 8 and Table 4.

3.6. MD simulation

The RMSD values of the acetylcholinesterase-β-sitosterol complex revealed time evaluation graphs of protein backbone deviations and variations during simulations. The complex stability was analysed from the simulation trajectory data (Fig. 9). The stability of the system is represented by a steady, low rate of change in the number of backbone atoms. The RMSD plot shows the minimum fluctuations in ligand bond system as compared to free state of acetylcholinesterase. The systems remained stable and attained the equilibrium during the 100 ns simulation trajectory (Fig. 9A). A slight fluctuation due to the system adjustment was seen that has been widely dispersed at 80 ns in RMSD.

The SASA (solvent-accessible surface area) of a protein molecule is the total surface area of the molecule that is accessible to the adjacent solvent and is necessary in study the stability and folding of specific protein. The SASA analysis and the presence of native contacts are substantial to recognize the protein folding. In this study the time evaluation of SASA of LOX-5 has been analysed before and after the binding of specific ligand β-sitosterol. It is depicted from the plot that during simulation, there is no major changing in the values of SASA. Moreover, in spite in the presence of β-sitosterol, the structure of LOX-5 is stable throughout the simulation (Fig. 9B). The SASA distribution follows a similar equilibration pattern which correlates with the Rg values and has no effect on the folding or compactness (Fig. 9B).

During MD simulations, the analysis of root-mean-square fluctuation (RMSF) is helpful for quantifying the residual vibrations in a protein molecule. The RMSF of the protein backbone was calculated for all systems (LOX-5-apo, LOX-5-β-sitosterol) to investigate the flexibility of residues. Fig. 9C illustrates that all systems have the same RMSF pattern and have steady and minimal residual fluctuations after β-sitosterol binding thus, defining the stability of the LOX-5-β-sitosterol complex. A limited number of residues in the LOX-5-β-sitosterol complex changed compared to apo-systems, indicating the binding adjustment during RMSD study. The fluctuation in the LOX-5 structure following β-sitosterol binding was found in the helix region. Therefore, RMSFs revealed that β-sitosterol form persistent interactions with LOX-5 during MD simulations.

The tertiary structure of a protein is intimately linked to its radius of gyration (Rg), which is the root-mean-square distance of a group of atoms from their collective centre of mass. The parameter Rg is extensively used to assess the compactness of a protein structure. The compactness of LOX-5 in both its apo and ligand-bound forms was evaluated by measuring its Rg values over time. During the simulation, the compactness was assessed (LOX-5-apo, LOX-5-β-sitosterol). Across the whole trajectory, LOX-5 remains stable between 1.90 and 2.05 nm as shown in (Fig. 9C) and maintains a constant structural dynamic and folding after β-sitosterol binding.

3.7. Hydrogen bond dynamic

The hydrophobic interactions and intramolecular hydrogen bonds (H-bonds) are significant in stabilizing the structural conformation in a protein. The presence of H-bonds within a protein plays a more crucial role in the overall folding, conformation, and compactness of the protein structure. By analysing the MD trajectories, we have studied the intramolecular H-bonds of acetylcholinesterase and their consistency with or

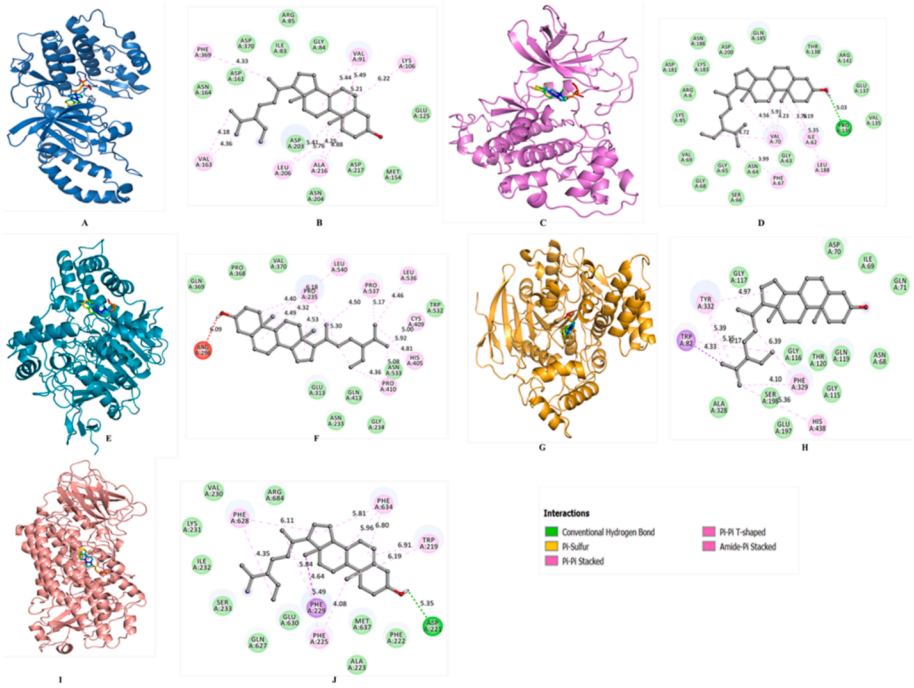

Fig. 8. Docking interactions of β-sitosterol with AD biomarkers (A and B) interaction of β-sitosterol with 4L6Q, (C and D) interaction of β-sitosterol with 4NM3, (E and F) interaction of β-sitosterol with 4p6Q, and (G and H) interaction of β-sitosterol with 6ESY, and (I and J) interaction of β-sitosterol with 6N2W.

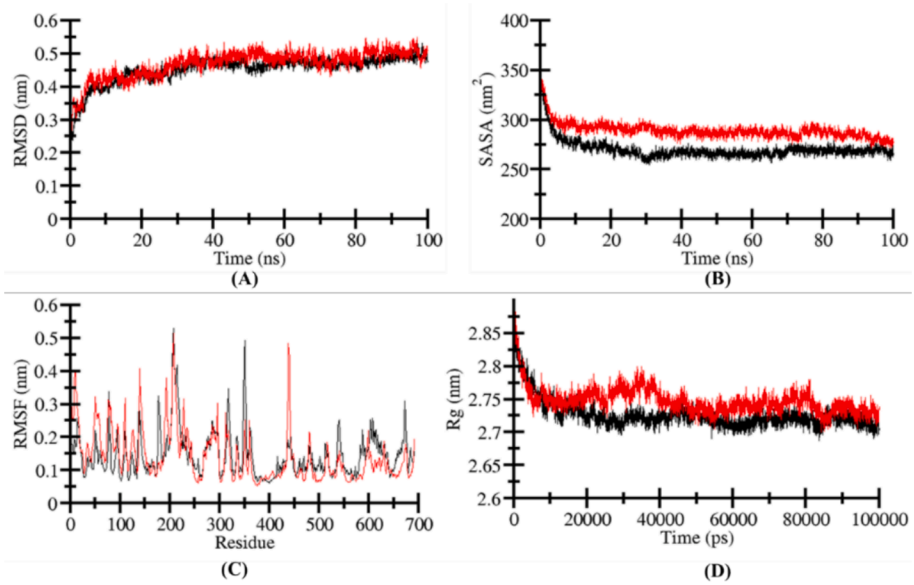

Fig. 9. Structural dynamics of apo-4NM3 (black) and β-sitosterol complex (red). (A) RMSD, (B) SASA values, (C) RMSF, and (D) Rg values across Cα backbone atoms of apo- and β-sitosterol and 6N2W complex calculated after 100 ns of MD trajectories.

without the binding of β-sitosterol with respect to time. The Fig. 8E and 8G shows the formation of the number of H-bonds and their fluctuation level within acetylcholinesterase before and after the binding of β-sitosterol. The graph indicates that H-bonds formed within Protein acetylcholinesterase were constant and this stability determine the structural confirmation of protein (Fig. 10A and 10C). The dynamic study also demonstrated that the Protein-ligand (acetylcholinesterase-β-sitosterol) complex were more compact than the apo-state of acetylcholinesterase due to an increase in intramolecular H-bonds.

3.7.1. Secondary structure changes in acetylcholinesterase and β-sitosterol complex

Alterations in the structural content of the acetylcholinesterase following β-sitosterol binding were quantified by calculating and analysing the secondary structural components. For each time step the residues of α-helix, β-sheet and turns in acetylcholinesterase were separated individually and the graph shows the number of residues involved in the formation of secondary structure. In the apo-state of acetylcholinesterase, its structural residues remain constant and at equilibrium during the entire process of simulation (Fig. 10B and 10D). There is a reduction in the α-helix and β-bridges of acetylcholinesterase in the presence of β-sitosterol. Moreover, there is also a slight reduction

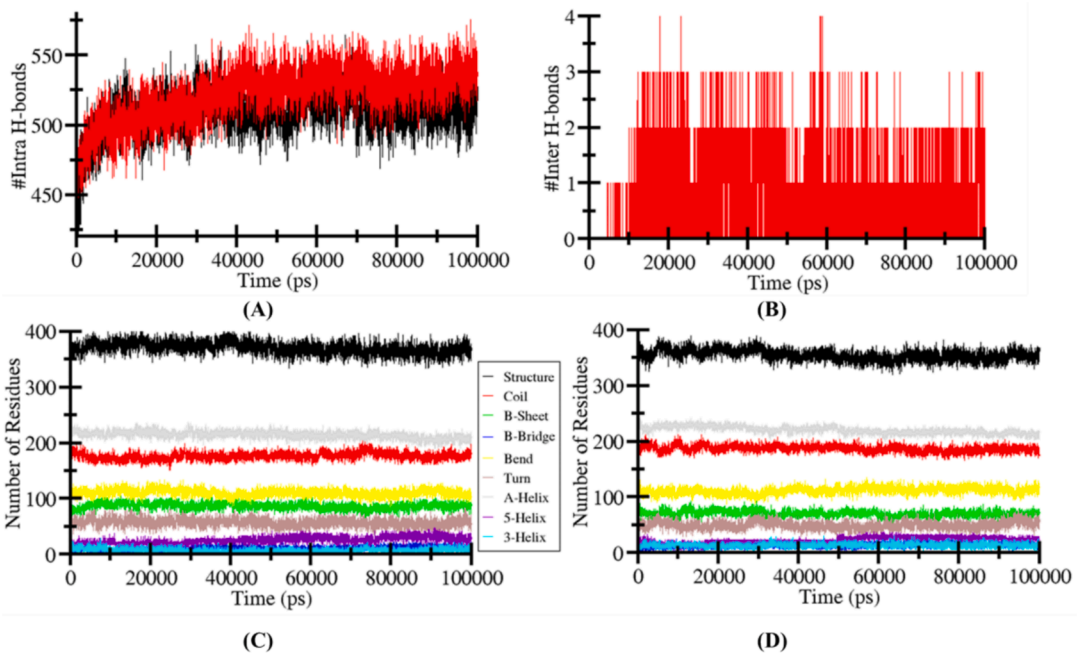

Fig. 10. Analysis of hydrogen bonding. (A) The apo-(black) and β-sitosterol-LOX-5 complex (red) exhibits intramolecular hydrogen bonds. (B) β-sitosterol-4NM3 complex exhibits intermolecular hydrogen bonding between its constituent molecules. (C and D) The quantity of residues determined following a 100 ns MD simulation, and the proportion of residues involved in the development of an average structure.

Table 5
Percentage of residues participated in average structure formation.

Complex	Percentage of protein secondary structure								
	Structure*	Coil	β-sheet	β-bridge	Bend	Turn	α-helix	5-helix	3-helix
6N2W	0.54	0.26	0.13	0.02	0.16	0.08	0.31	0.04	0.01
LOX-βS	0.51	0.27	0.10	0.02	0.16	0.07	0.32	0.03	0.02

in secondary structure residues in acetylcholinesterase −β-sitosterol complex state due to the formation of turn, bend, and helix. (Fig. 10B and 10D and Table 5). The strong stability of the complex is supported by the fact that acetylcholinesterase secondary structure didn't change much upon β-sitosterol binding.

4. Discussion

Plants are being evaluated against different diseases due to their substantial biological activities. This is because natural products have a higher margin of safety than synthetic pharmaceuticals, making them a more attractive option for usage as therapeutic agents (Sen et al., 2010). The presence of different classes of phytochemicals, including phenolic and flavonoid compounds acts as scavengers of free-radical, reducing molecules, and suppress the production of singlet-oxygen (Andlauer and Fürst, 1998). β-sitosterol is a phytosterol and possesses different biological properties. β-sitosterol has shown significant *in vitro* antioxidant activities. These activities of β-sitosterol might be due to the hydroxyl (OH). Moreover, several other studies have also supported this finding as β-sitosterol isolated from *Arisaema utile* also showed substantial antioxidant activity (Bhat et al., 2019).

The aetiology of AD is strongly correlated with oxidative stress (Sajad et al., 2022). The loss of synapses and neurons is a key step in the advancement of AD, and oxidative stress plays a role in this by stimulating the deposition of NFTs and β-amyloids. Neuronal components (proteins, lipids, and nucleic acids) are all vulnerable to oxidative stress in AD, leading to mitochondrial failure, elevated metal concentrations, inflammation, NFTs, and peptides of β-amyloid (Chen and Zhong 2014). It is well-known that metals induce neurodegeneration by inducing oxidative stress, and in recent years, $AlCl_3$ has been consistently connected to neurological disorders, including AD. It is associated with the formation and fibrillization of Aβ in AD brains. In addition, $AlCl_3$ is known to increase the concentration of Aβ and NFT in the brain tissues of treated rats (Liu et al., 2019). $AlCl_3$ accumulates in the brain through absorptions across the blood–brain barrier (BBB), particularly in the hippocampus, which is important for learning and memory formation. Long-term accumulated growth of $AlCl_3$ stimulates neurotoxicity via neurofibrillary tangles and amyloid aggregation. Several investigations have demonstrated that AD is related to enhanced $AlCl_3$ levels in the brain (Thenmozhi et al., 2015). Understanding the mechanism of $AlCl_3$-generated neurotoxicity is crucial because no cure or therapy is readily available for AD. $AlCl_3$ exposure causes neurochemical changes that impair memory and learning in animals. In recent years, phytochemicals have been used to treat several disorders. As there is no cure or therapy for AD, it's crucial to understand how $AlCl_3$ produces neurotoxicity. Most phytochemicals, particularly polyphenolic, flavonoid, and alkaloid compounds, have received attention for treating numerous disorders (Sajad et al., 2020, Ali et al., 2022). Recent studies suggest that catechins, curcumin, and resveratrol have slowed down how AD develops and worsens. They can reduce inflammation, protect cells from free radical damage, and prevent amyloid beta formation (Kim et al., 2010, Velmurugan et al., 2018, Ahmed et al., 2022). As a result, we have designed a study to determine how β-sitosterol from the *Asplenium caudatum* plant affected the rat AD model induced by using $AlCl_3$. To study the impact on extinction learning and associative memory, $AlCl_3$ was administered intraperitoneally, and the behaviors of the experimental rats were observed. $AlCl_3$ caused the loss of neurons and their function in the hippocampal region, making it harder for the rats to

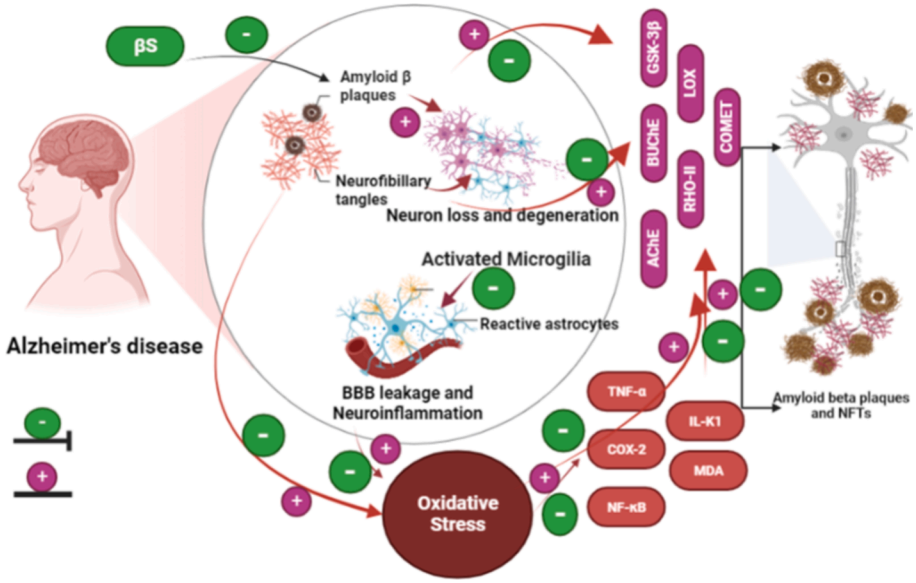

Fig. 11. Schematic representation of mechanistic approach of compound β-sitosterol against the pathophysiology of AD by suppressing its associated pathways.

recall and remember where the escaped platform was in Z maze tests. Interestingly, treatment with β-sitosterol has reversed the effect of $AlCl_3$ in the brain and enhanced the spatial memory and learning capacity in experimental rats. Previous research has shown that *methylphenidate* and *rosmarinus officinalis* (Khalid et al., 2020), *Syzygium aromaticum* (Amber et al., 2018), and *Vitis vinifera* (Borai et al., 2017) improve memory in the $AlCl_3$-induced neurotoxicity mice model. As a result, it's possible that β-sitosterol enhanced spatial memory thus, directing the substantial potential of the compound.

$AlCl_3$ has devastating effects on the functional characteristics of the membrane and indirectly causing oxidative damage to membrane lipids and an imbalance among antioxidant and prooxidant defense mechanism (Sajad and Thakur 2018, Firdaus et al., 2022). The oxidative stress generated by the i.p injection of $AlCl_3$ in the AD brain was reflected in elevated levels of MDA, Nitric oxide, and reduced production of CAT and SOD enzymes and level of GSH. However, the β-sitosterol treatment reduced the MDA and NO levels and increased the level of GSH and activity of CAT and SOD enzymes both in the cerebral cortex and hippocampus regions of the brain (Sumathi et al., 2013). Several phytochemicals like quercetin (Al-Otaibi et al., 2018), etodolac (Singh et al., 2014), and resveratrol (Al-Bishri et al., 2017) other active herbal substances have been discovered to reduce $AlCl_3$-induced oxidative stress by increasing the natural antioxidant mechanisms. Therefore, our results prove that β-sitosterol has neuroprotective properties in an $AlCl_3$-induced rat model due to its antioxidant effect.

Oxidative stress contributes to cholinergic dysfunction by damaging cholinergic neurons and impairing acetylcholine synthesis and release, which are critical for cognitive function. This disruption accelerates neurodegeneration in conditions like Alzheimer's disease, where cholinergic deficits are prominent (Prabha et al., 2024). The cholinergic hypothesis is the earlier hypothesis about the pathophysiology of AD, and it is fundamental to the pathogenesis of AD. It is well accepted that the excitatory neurotransmitter acetylcholine (ACh) and butyrylcholine, respectively (BuCh) have a vital role in learning, memory, and other complex actions. The cholinergic nervous system in the brain may impact the level of Ach and BuCh by controlling its production and secretion (Giacobini et al., 2022). AChE maintains the membrane integrity of cholinergic neurons via transmembrane protein (Na^+K^+ ATPase) activity. Cholinergic transmission failure is a contributing factor in the memory impairment in AD. The alteration in cholinergic transmission occurs due to the changes in blood–brain barrier (BBB) system by $AlCl_3$, due to its effective cholino-toxic nature, (Thenmozhi et al., 2015, Rather et al., 2018). Rutin protects the Cu-induced brain injury by lowering the observed histological change and enhancing inflammatory and antioxidant indicators through antioxidative and anti-inflammatory mechanisms (Arowoogun et al., 2021). The treatment of $AlCl_3$ in rats leads to a considerable rise in AChE intensity and activity of the transmembrane protein in the current investigation. Treatment of rats with β-sitosterol lowered the level of AChE, BuChE, GSK-3β, Rho-II, and Lipoxygenase-5 enzymes along with a decrease in the activity of the transmembrane protein, which is consistent with other research. This study presented evidence that β-sitosterol promotes neuroprotection by inhibiting the synthesis, release, and activity of enzymes that promote the progression and development of AD.

Chronic inflammation is increasingly recognized as a key driver in the pathogenesis of AD, contributing to neuronal damage and cognitive decline (Andlib et al., 2024, Prabha et al., 2024). The pathogenicity of early-stage AD is mostly attributable to the inflammatory response (Akiyama et al., 2000). Inflammation involves the activation of many genes through a complicated regulatory network, including various transcription factors and cytokines (Rogers et al., 1996). The chronic production of TNF-α and COX-2 by microglia induces a neuroinflammatory response that has been related to AD and other degenerative disorders (Medeiros and LaFerla 2013, Dong et al., 2022). The aggregation of Aβ plaques and tau protein hyperphosphorylation in the brain tissue is also facilitated by TNF-α and COX-2-associated inflammation. The degree of TNF-α and COX-2 expression was considerably elevated in $AlCl_3$-induced rats, but after the treatment of β-sitosterol dose-dependently reduced the activity of both TNF-α and COX-2. This result has also been supported by previous studies carried out on plant extracts (Sun et al., 2020, Tan et al., 2022) and individual phytochemicals such as rutin (Sun et al., 2021), orientin (Qu et al., 2022), and resveratrol (Huang et al., 2021).

Histopathological examination of $AlCl_3$ toxicity found that it leads to neuronal loss and death, the activation of inflammatory indicators, and the destruction of vacuoles due to oxidative stress, inflammation, and deterioration in the antioxidant defense system. By decreasing the $AlCl_3$-induced toxicity, the compound β-sitosterol treatment improves neuronal cellular structure and function by reducing the synthesis and expression of AD biomarkers.

Moreover, the molecular docking studies also revealed that β-sitosterol had shown a substantial affinity towards AD-associated biomarkers. The MD simulation study also confirms the strong stability of target proteins after binding ligands.

Many phytochemicals demonstrate potential in treating AD. β-sitosterol's unique combination of anti-inflammatory and antioxidant properties, along with its ability to reduce AD-associated biomarkers and oxidative stress, positions it as a particularly compelling candidate. The multifaceted approach of β-sitosterol addresses several key pathological processes in AD, setting it apart from other phytochemicals that may only target one or two of these pathways (Fig. 11). Additionally, β-sitosterol's superior bioavailability compared to other phytochemicals enhances its potential as a therapeutic agent for AD.

5. Conclusions

The research described above demonstrates conclusively that β-sitosterol is an effective pharmacological drug capable of minimizing neurological deficits and preventing subsequent damage caused by $AlCl_3$-induced toxicity. It also enhanced the cholinergic function along with the suppression of GSK-3β, Rho-II, lipoxygenase, and Na^+K^+ ATPase and the generation of oxidative stress induced through the activation of the inflammatory biomarkers like TNF-α and COX-2, which may be due to the potent antioxidant action of β-sitosterol. Moreover, molecular dynamic studies also confirm the strong affinity of β-sitosterol towards the biomarkers of AD. These findings indicate that β-sitosterol may be a potential therapeutic agent for the prevention and treatment of neurodegenerative diseases. Although β-sitosterol has shown promising efficacy in this study, further research is needed to confirm its anti-Alzheimer's activity in different AD models.

Ethical approval

The study was approved by the Institutional Animal Ethical Committee, National Institute of Health and Family Welfare Munirka, New Delhi, under the reference of (Item No. 19.1) 2021.

CRediT authorship contribution statement

Mohd Sajad: Writing – review & editing, Writing – original draft, Visualization, Validation, Software, Resources, Methodology, Conceptualization. **Rafat Ali:** Software, Data curation. **Rajesh Kumar:** Supervision. **Nida Jamil khan:** Software. **Shadma Wahab:** Investigation, Funding acquisition. **Saad Ali Alshehri:** Investigation, Funding acquisition. **Sonu Chand Thakur:** Writing – review & editing, Supervision, Conceptualization.

Declaration of competing interest

The authors declare that they have no known competing financial interests or personal relationships that could have appeared to influence the work reported in this paper.

Acknowledgments

The authors are thankful to the National Institute of Health and Family Welfare for providing the animal facility and to CSIR-UGC Net JRF Fellowship, New Delhi, India, for providing financial assistance to Mohd Sajad, under the guidance of Dr. Sonu Chand Thakur, for carrying out this research work. The authors also extend their appreciation to the Deanship of Research and Graduate Studies at King Khalid University for funding this work through the Large-Scale Research Project under grant number RGP2/274/45.

References

Abraham, M.J., Murtola, T., Schulz, R., et al., 2015. GROMACS: High performance molecular simulations through multi-level parallelism from laptops to supercomputers. *SoftwareX* 1, 19–25.

Ahmed, M.M., Tazyeen, S., Haque, S., et al., 2022b. Network-based approach and IVI methodologies, a combined data investigation identified probable key genes in cardiovascular disease and chronic kidney disease. *Front. Cardiovasc. Med.* 8, 755321.

Ahmed, M., Verma, A.K., Patel, R., et al., 2022a. Physiochemical, antioxidant, and food simulant release properties of collagen-carboxymethyl cellulose films enriched with Berberis lyceum root extract for biodegradable active food packaging. *J. Food Process. Preserv.* 46, e16485.

Akiyama, H., Barger, S., Barnum, S., et al., 2000. Inflammation and Alzheimer's disease. *Neurobiol. Aging* 21, 383–421.

Al-Bishri, W.M., Hamza, A.H., Farran, S.K., et al., 2017. Resveratrol Treatment Attenuates Amyloid Beta, Tau Protein and Markers of Oxidative Stress, and Inflammation in Alzheimer's disease Rat Model. *International Journal of Pharmaceutical Research & Allied Sciences* 6 (3).

Ali, A., Zahid, H.F., Cottrell, J.J., et al., 2022. A comparative study for nutritional and phytochemical profiling of coffea arabica (C. arabica) from different origins and their antioxidant potaluminum chloride-inducedential and molecular docking. *Molecules* 27 (16) (2022), 5126.

Al-Otaibi, S.S., Arafah, M.M., Sharma, B., et al., 2018. Synergistic effect of quercetin and α-lipoic acid on aluminium chloride induced neurotoxicity in rats. *Journal of Toxicology* 2018 (1), 281703.

Amber, S., Shah, S.A.A., Ahmed, T., et al., 2018. Syzygium aromaticum ethanol extract reduces AlCl3-induced neurotoxicity in mice brain through regulation of amyloid precursor protein and oxidative stress gene expression. *Asian Pac. J. Trop. Med.* 11 (2), 123–130.

N. Andlib M. Sajad R. Kumar et al. Abnormalities in sex hormones and sexual dysfunction in males with diabetes mellitus: A mechanistic insight. 125 2023 151974.

Andlib, N., Sajad, M., Thakur, S.C., 2024. Association of diabetes mellitus with risk of reproductive impairment in females: A comprehensive review. *Acta Histochem.* 125 (1) (2023), 151974.

Arowoogun, J., Akanni, O.O., Adefisan, A.O., et al., 2021. Rutin ameliorates copper sulfate-induced brain damage via antioxidative and anti-inflammatory activities in rats. *J. Biochem. Mol. Toxicol.* 35 (1), e22623.

Baba, S.A., Malik, S.A., 2015. Determination of total phenolic and flavonoid content, antimicrobial and antioxidant activity of a root extract of Arisaema jacquemontii Blume. *Journal of Taibah University for Science* 9 (4), 449–454.

Babatunde, J.O., Kayode, O.K., 2019. Inhibitory action of dried leaf of Cassia alata (Linn.) Roxb against lipoxygenase activity and nitric oxide generation. *Scientia Agropecuaria* 10 (2), 185–190.

Babu, S., Jayaraman, S., 2020. An update on β-sitosterol: A potential herbal nutraceutical for diabetic management. *Biomed. Pharmacother.* 131, 110702.

Bhat, A.H., Alia, A., Rather, G.M., et al., 2019. Isolation & characterisation of beta-sitosterol from the rhizomes of Arisaema utile and its evaluation for antioxidant activity. *Int. J. Sci. Res. Biol. Sci.* 6, 111–118.

Borai, I.H., Ezz, M.K., Rizk, M.Z., et al., 2017. Therapeutic impact of grape leaves polyphenols on certain biochemical and neurological markers in AlCl3-induced Alzheimer's disease. *Biomed. Pharmacother.* 93, 837–851.

Chen, Z., Zhong, C., 2014. Oxidative stress in Alzheimer's disease. *Neurosci. Bull.* 30, 271–281.

Dong, S., Duan, Y., Hu, Y., et al., 2012. Advances in the pathogenesis of Alzheimer's disease: a re-evaluation of amyloid cascade hypothesis. Transl Neurodegener, BioMed Central Ltd. *Translational neurodegeneration. J. Neuroinflammation* 19 (1), 205.

Dong, Y., Yu, H., Li, X., et al., 2022. Hyperphosphorylated tau mediates neuronal death by inducing necroptosis and inflammation in Alzheimer's disease. *J. Neuroinflammation* 19 (1), 205.

Ellman, G.L., 1959. Tissue sulfhydryl groups. *Arch. Biochem. Biophys.* 82 (1), 70–77.

Ellman, G.L., Courtney, K.D., Andres Jr, V., et al., 1961. A new and rapid colorimetric determination of acetylcholinesterase activity. *Biochem. Pharmacol.* 7 (2), 88–95.

Farooqui, A.A., Farooqui, T., Madan, A., et al., 2018. Ayurvedic medicine for the treatment of dementia: mechanistic aspects. *Evidence-based Complementary and Alternative Medicine* 2018 (1), 2481076.

Firdaus, Z., Kumar, D., Singh, S.K., et al., 2022. Centella asiatica Alleviates AlCl3-induced Cognitive Impairment, Oxidative Stress, and Neurodegeneration by Modulating Cholinergic Activity and Oxidative Burden in Rat Brain. *Biol. Trace Elem. Res.* 200 (12), 5115–5126.

Giacobini, E., Cuello, A.C., Fisher, A.J.B., 2022. Reimagining cholinergic therapy for Alzheimer's disease. *Brain* 145 (7), 2250–2275.

Green, L.C., Wagner, D.A., Glogowski, J., et al., 1982. Analysis of nitrate, nitrite, and [15N] nitrate in biological fluids. *Anal. Biochem.* 126 (1), 131–138.

Grossberg, G.T., Christensen, D.D., Griffith, P.A., et al., 2010. The art of sharing the diagnosis and management of Alzheimer's disease with patients and caregivers: recommendations of an expert consensus panel. *The Primary Care Companion for CNS Disorders* 12 (1), 26659.

Hejazi, I.I., Khanam, R., Mehdi, S.H., et al., 2017. New insights into the antioxidant and apoptotic potential of Glycyrrhiza glabra L. during hydrogen peroxide mediated oxidative stress: an in vitro and in silico evaluation. *Biomed. Pharmacother.* 94, 265–279.

Huang, L., He, Z., Guo, L., et al., 2008. Improvement of cognitive deficit and neuronal damage in rats with chronic cerebral ischemia via relative long-term inhibition of rho-kinase. Cellular and molecular neurobiology. *Cell. Mol. Neurobiol.* 28, 757–768.

Huang, J., Huang, N., Xu, S., et al., 2021. Signaling mechanisms underlying inhibition of neuroinflammation by resveratrol in neurodegenerative diseases. *J. Nutr. Biochem.* 88, 108552.

Huang, W.J., Zhang, X., Chen, W.W., 2016. Role of oxidative stress in Alzheimer's disease. Biomed Rep. 4, 519–522.

Johnson, D.K., Storandt, M., Morris, J.C., et al., 2008. Cognitive profiles in dementia: Alzheimer disease vs healthy brain aging. Neurology*Neurology* 71 (22), 1783–1789.

Khalid, A., Abbasi, U.A., Amber, S., et al., 2020. Methylphenidate and Rosmarinus officinalis improves cognition and regulates inflammation and synaptic gene expression in AlCl3-induced neurotoxicity mouse model. *Mol. Biol. Rep.* 47, 7861–7870.

Kim, J., Lee, H.J., Lee, K.W., 2010. Naturally occurring phytochemicals for the prevention of Alzheimer's disease. *J. Neurochem.* 112 (6), 1415–1430.

Liaquat, L., Muddasir, S., Batool, Z., et al., 2017. Development of AD like symptoms following co-administration of AlCl3 and D-gal in rats: A neurochemical, biochemical and behavioural study. *Pak. J. Pharm. Sci.* 30(2 (Suppl.)), 647.

Liu, P.-P., Xie, Y., Meng, X.-Y., et al., 2019. History and progress of hypotheses and clinical trials for Alzheimer's disease. *Signal Transduct. Target. Ther.* 4 (1), 29.

Marklund, S., Marklund, G., 1974. Involvement of the superoxide anion radical in the autoxidation of pyrogallol and a convenient assay for superoxide dismutase. *Eur. J. Biochem.* 47 (3), 469–474.

Medeiros, R., LaFerla, F.M., 2013. Astrocytes: conductors of the Alzheimer disease neuroinflammatory symphony. *Exp. Neurol.* 239, 133–138.

Mehla, J., Pahuja, M., Dethe, S.M., et al., 2012. Amelioration of intracerebroventricular streptozotocin induced cognitive impairment by Evolvulus alsinoides in rats: in vitro and in vivo evidence. *Neurochem. Int.* 61 (7), 1052–1064.

Mohamed, T.M., Youssef, M.A.M., Bakry, A.A., et al., 2021. Alzheimer's disease improved through the activity of mitochondrial chain complexes and their gene expression in rats by boswellic acid. Metab. Brain Dis.*Metabolic Brain Disease* 36, 255–264.

Monczor, M., 2005. Diagnosis and treatment of Alzheimer's disease. *Current Medicinal Chemistry-Central Nervous System Agents* 5 (1), 5–13.

Morris, R., 1984. Developments of a water-maze procedure for studying spatial learning in the rat. *J. Neurosci. Methods* 11 (1), 47–60.

Mousavi-Nasab, K., Amani, M., Mostafalou, S., 2024. The Effect of Trientine on Alcl3-Induced Cognitive Dysfunction and Biochemical Changes in the Hippocampus of Rats. *Drug Research* 74 (08), 405–414.

Nirala, R. K., P. Dutta, M. Z. Malik, et al., 2019. In vitro and in Silico evaluation of Betulin on calcium oxalate crystal formation. *Journal of the American College of Nutrition* 38.7 (2019): 586-596.

Ohkawa, H., Ohishi, N., Yagi, K., 1979. Assay for lipid peroxides in animal tissues by thiobarbituric acid reaction. *Anal. Biochem.* 95 (2), 351–358.

Prabha, S., Sajad, M., Hasan, G.M., et al., 2024. Recent advancement in understanding of Alzheimer's disease: Risk factors, subtypes, and drug targets and potential therapeutics. *Ageing Res. Rev.* 102476.

Qu, Y., Shi, L., Liu, Y., et al., 2022. Orientin Prolongs the Longevity of Caenorhabditis elegans and Postpones the Development of Neurodegenerative Diseases via Nutrition Sensing and Cellular Protective Pathways. *Oxid. Med. Cell. Longev.* 2022 (1), 8878923.

Rather, M.A., Thenmozhi, A.J., Manivasagam, T., et al., 2018. Neuroprotective role of Asiatic acid in aluminium chloride induced rat model of Alzheimer's disease. *Front Biosci (schol Ed)* 10 (2), 262–275.

Rogers, J., Webster, S., Lue, L.-F., et al., 1996. Inflammation and Alzheimer's disease pathogenesis. *Neurobiol. Aging* 17 (5), 681–686.

Sajad, M., Ahmed, M.M., Thakur, S.C., 2022. An integrated bioinformatics strategy to elucidate the function of hub genes linked to Alzheimer's disease. *Gene Reports* 26, 101534.

Sajad, M., Kumar, R., Thakur, S.C., 2022. History in Perspective: The Prime Pathological Players and Role of Phytochemicals in Alzheimer's Disease. *IBRO Neuroscience Reports* 12, 377–389.

Sajad, M., Thakur, S.C., 2018. Traditional Uses and Anti-Inflammatory Activities of Different Medicinal Plants: A Systematic Review. I*Nt. J. Ayurvedic Herb. Med* 9, 3410–3432.

Sajad, M., Thakur, S.C., 2020. Occurrence and bioactivity of phytochemicals and their role in human health. Adv, Health Dis., p. 83

Siddiqui, A., Akhtar, S., Shah, Z., et al., 2021. Inflammation Drives Alzheimer's Disease: Emphasis on 5-lipoxygenase Pathways. Curr. Neuropharmacol.*Current Neuropharmacology* 19 (6), 885–895.

Singh, M., Prashar, Y., 2020. Cerebral Cortex and Hippocampal Protection Mediated by Callistemon viminalis in Aluminium Chloride Induced Alzheimer's Disease. INDIAN JOURNAL OF PHARMACEUTICAL EDUCATION AND RESEARCH. *Indian J. Pharm. Educ. Res* 54 (2), 422–431.

Singh, S., Singh, R., Kushwah, A.S., et al., 2014. Neuroprotective role of antioxidant and pyranocarboxylic acid derivative against AlCl3 induced Alzheimer's disease in rats. *J Coast Life Med* 2 (7), 571–578.

Small, G.W., 2002. Structural and functional brain imaging of alzheimer disease. The Fifth Generation of Progress, Neuropsychopharmacology, pp. 1232–1242.

Sperling, R.A., Aisen, P.S., Beckett, L.A., et al., 2011. Toward defining the preclinical stages of Alzheimer's disease: Recommendations from the National Institute on Aging-Alzheimer's Association workgroups on diagnostic guidelines for Alzheimer's disease. *Alzheimers Dement.* 7 (3), 280–292.

Sumathi, T., Shobana, C., Mahalakshmi, V., et al., 2013. Oxidative stress in brains of male rats intoxicated with aluminium and neuromodulating effect of Celastrus paniculatus alcoholic seed extract. *Asian J Pharm Clin Res* 6 (3), 80–90.

Sun, X.-Y., Li, L.-J., Dong, Q.-X., et al., 2021. Rutin prevents tau pathology and neuroinflammation in a mouse model of Alzheimer's disease. *J. Neuroinflammation* 18 (1), 131.

Sun, J., Xu, J., Yang, B., et al., 2020. Effect of Clostridium butyricum against microglia-mediated neuroinflammation in Alzheimer's disease via regulating gut microbiota and metabolites butyrate. *Mol. Nutr. Food Res.* 64 (2), 1900636.

Tan, B., Wang, Y., Zhang, X., et al., 2022. Recent Studies on Protective Effects of Walnuts against Neuroinflammation. *Nutrients* 14 (20), 4360.

Thenmozhi, A.J., Raja, T.R.W., Janakiraman, U., et al., 2015. Neuroprotective effect of hesperidin on aluminium chloride induced Alzheimer's disease in Wistar rats. *Neurochem. Res.* 40, 767–776.

Trott, O., Olson, A.J.J., 2010. AutoDock Vina: improving the speed and accuracy of docking with a new scoring function, efficient optimization, and multithreading. *J. Comput. Chem.* 31 (2), 455–461.

Velmurugan, B.K., Rathinasamy, B., Lohanathan, B.P., et al., 2018. Neuroprotective role of phytochemicals. *Molecules* 23 (10), 2485.